The Fluctuating Two-Ray Fading Model with Independent Specular Components

Maryam Olyaee, José A. Cortés, F. Javier Lopez-Martinez, José F. Paris and Juan M. Romero-Jerez

***Abstract*—We introduce and characterize the independent fluctuating two-ray (IFTR) fading model, a class of fading models consisting of two specular components which fluctuate *independently*, plus a diffuse component modeled as a complex Gaussian random variable. The IFTR model complements the popular fluctuating two-ray (FTR) model, on which the specular components are fully correlated and fluctuate *jointly*. The chief probability functions of the received SNR in IFTR fading, including the PDF, CDF and MGF, are expressed in closed-form, having a functional form similar to other state-of-the-art fading models. Then, the IFTR model is empirically validated using multiple channels measured in rather diverse scenarios, including line of sight (LOS) millimeter-wave, land mobile satellite (LMS) and underwater acoustic communication (UAC), showing a better fit than the original FTR model and other models previously used in these environments. Additionally, the performance of wireless communication systems operating under IFTR fading is evaluated in closed-form in two scenarios: (*i*) exact and asymptotic bit error rate for a family of coherent modulations; and (*ii*) exact and asymptotic outage probability.**

***Index Terms*—Wireless channel modeling, moment generating function, multipath propagation, small-scale fading, two-ray, fluctuation.**

I. Introduction

SMALL-SCALE fading is a key propagation effect in many wireless scenarios. The accurate modeling of this phenomenon in the millimeter-wave (mmWave) band has become particularly relevant because of its use in the fifth generation (5G) standard. This also applies to land mobile satellite (LMS) channels, which are attracting an increasing interest as the sixth generation (6G) standard is expected to integrate space-ground links to provide global coverage [1]. This propagation phenomenon also occurs even in environments where information is conveyed by means of non-electromagnetic waves, as in underwater acoustic communications (UAC) [2].

The Rice distribution has been largely employed to model line of sight (LOS) wireless channels. Recent attempts to characterize fading in mmWave channels, for instance, have used it [3], [4]. Two refinements of the Rice model are of particular interest because of their relevant physical interpretation: one considers that the LOS (or specular) component considered in the Rice model fluctuates randomly. This yields the Rician-shadowed distribution, which has been employed to model LMS channels [5]. The second one considers an additional specular component, yielding the two-wave with diffuse power (TWDP) model [6], [7], which has proven to outperform the Rice distribution when modeling indoor channels at 60 GHz [8].

The fluctuating two-ray (FTR) model was recently proposed as a natural generalization of *both* the Rician-shadowed and the TWDP models, and many others [9]. It consists of two specular components with random phases that jointly fluctuate, plus a diffuse component. The chief probability functions - cumulative density function (CDF), probability density function (PDF) and moment generating function (MGF) - of the FTR model can be expressed in closed-form and the model provides a good fit to mmWave field measurements. Thus, it has been used for the performance analysis of cellular networks in the mmWave band [10] and it has been considered in a recently proposed channel classification scheme for 5G mobile communications networks [11]. Moreover, an effective parameter estimation technique has been shown to be feasible for the FTR model [12].

The FTR fading model assumes the simultaneous fluctuation of the two specular components, which will typically occur when the scatterers are close to the transmitter and/or the receiver, or when the specular components are totally or partially blocked by the same obstacle. However, there are some wireless scenarios, relevant in practical situations, where the specular components follow very different paths and are affected by different scatterers and/or disturbances. This is for example the case when there is a direct path between the transmitter and receiver and also a strong reflected wave reaches the receiver experiencing significant fluctuations due to the movements of surrounding objects/reflectors, e.g., nearby flat objects in LOS urban cellular communications; or due to the varying nature of the reflecting surfaces as transmitter and receiver move, such as the ocean surface in maritime RF communications [13] and in underwater acoustic communications [2]. Similarly, specular components following different paths also experience dissimilar fluctuations when the medium is inhomogeneous, as in underwater acoustic communications, where the temperature gradient and undersea currents cause different propagation conditions for the direct and reflected paths. In these situations, the almost negligible fluctuation of the direct-path link, as opposed to the often much stronger fluctuation of the reflected wave (as we will later show in the fitting of experimental data) generally suggests that the

The authors are with Communications and Signal Processing Lab, Instituto Universitario de Investigación en Telecomunicación (TELMA), Universidad de Málaga, CEI Andalucía TECH. ETSI Telecomunicación, Bulevar Louis Pasteur 35, 29010, Málaga, Spain. M. Olyaee and F.J. Lopez Martinez are also with the Department of Signal Theory, Networking and Communications, Universidad de Granada, 18071, Granada, Spain.(e-mails: olyaee@ugr.es, jaca@ic.uma.es, paris@ic.uma.es, fjlm@ugr.es, romero@dte.uma.es).

This work has been funded in part by the Spanish Government and the European Fund for Regional Development FEDER (project TEC2017-87913-R), by Junta de Andalucía (projects P18-RT-3175, P18-PT-3587 and ProyExcel_00420) and by Universidad de Málaga (project UMA20-FEDERJA-002).

specular components will be highly uncorrelated, and may be considered independent for practical purposes.

Besides capturing the reality of a number of propagation mechanisms, allowing the specular components to fluctuate *independently* provides an additional degree of freedom that results in an improved modeling of these scenarios, which can be quite significant in some cases. For instance, in terms of the CDF, this is translated into an increased flexibility to change its log-log concavity and convexity, yielding a better fit to experimental data.

A special case of this scenario was originally suggested in [9], where the two specular components undergo independent and identically distributed (iid) Nakagami-m fluctuations. However, a thorough statistical characterization and analysis was not presented, and has never been carried out in the literature to the best of our knowledge. In this paper, we introduce, characterize and validate the independent fluctuating two-ray (IFTR) fading model to complement the FTR model by allowing the specular components to fluctuate independently and experience dissimilar fading severity, i.e., the specular components fluctuate according to non-necessarily identical distributions. Specifically, the following key contributions are made in this context:

- Expressions for the PDF, CDF, and MGF of the received power envelope, or equivalently the signal-to-noise ratio (SNR), under IFTR fading are obtained. It is worth noting that the IFTR model analytical derivations present new mathematical challenges, as the chief probability functions expressions must be obtained from a double integration due to the averaging over each of the two specular components. In spite of that, it is shown that these functions can be expressed in closed-form, having a functional form similar to other state-of-the-art fading models.
- It is shown that the IFTR model fits measured channels in rather diverse scenarios such as mmWave, LMS and UAC better than the FTR model and other models previously used in these environments.
- The performance of communication systems operating in these propagation conditions is analyzed, in terms of the exact and asymptotic bit error rate (BER) for a family of modulations, and in terms of the outage probability.
- The influence of the model parameters on the fading statistics and on the system performance is investigated, and the key differences with respect to the FTR model are assessed.

The remainder of this paper is organized as follows. Section II presents the physical channel model for the IFTR fading. Its statistical characterization in terms of the MGF, PDF, and CDF of the received SNR is carried out in Section III. Section IV shows the empirical validation of the newly proposed IFTR fading model. Based on the obtained statistical functions, performance analysis of wireless communications systems undergoing IFTR fading is exemplified in Section V. Numerical results are given in Section VI, and the main conclusions and remarks are summarized in Section VII.

II. Channel model

Let us assume that the small-scale fluctuations in the amplitude of a signal transmitted over a wireless channel are given by two fluctuating dominant waves, referred to as specular components[1], to which other diffusely propagating waves are added. The complex baseband voltage of the wireless channel of this model can be expressed as

$$V_r = \sqrt{\zeta_1}V_1 \exp(j\phi_1) + \sqrt{\zeta_2}V_2 \exp(j\phi_2) + X + jY, \quad (1)$$

where $\sqrt{\zeta_i}V_i \exp(j\phi_i)$ represents the *i-th* specular component ($i = 1, 2$), which is assumed to have an average amplitude V_i modulated by a random variable $\sqrt{\zeta_i}$ responsible for its fluctuation, where ζ_1 and ζ_2 are independent unit-mean Gamma distributed random variables with PDF

$$f_{\zeta_i}(u) = \frac{m_i^{m_i} u^{m_i-1}}{\Gamma(m_i)} e^{-m_i u}, \qquad i = 1, 2. \quad (2)$$

Without any loss of generality, in the sequel we will assume $V_1 \geq V_2$. The *i-th* specular component is assumed to have a uniformly distributed random phase ϕ_i, such that $\phi_i \sim \mathcal{U}[0, 2\pi)$, with ϕ_1 and ϕ_2 considered to be statistically independent. On the other hand, $X+jY$ is a complex Gaussian random variable, such that $X, Y \sim \mathcal{N}(0, \sigma^2)$, representing the diffuse received signal component due to the combined reception of numerous weak, independently-phased scattered waves. This model will be referred to as the IFTR fading model. Note that if $m_1, m_2 \to \infty$ then $\zeta_1, \zeta_2 \to 1$, i.e., the fluctuation of the specular components tends to disappear and the IFTR model tends to the TWDP fading model proposed by Durgin, Rappaport and De Wolf [6], also known as the Generalized Two-Ray fading model with Uniformly distributed phases (GTR-U) [7].

As with the TWDP fading model, the IFTR channel model can conveniently be described in terms of the parameters K and Δ, defined as

$$K \triangleq \frac{V_1^2 + V_2^2}{2\sigma^2}, \quad (3)$$

$$\Delta \triangleq \frac{2V_1V_2}{V_1^2 + V_2^2}, \quad (4)$$

where the parameter K represents the ratio of the average power of the dominant (specular) components to the power of the remaining diffuse multipath. On the other hand, Δ is a parameter ranging from 0 to 1 capturing how similar to each other are the average received powers of the specular components: when the average magnitudes of the two specular components are equal, we have $\Delta = 1$. Conversely, in the absence of a second component ($V_1 = 0$ or $V_2 = 0$), then $\Delta = 0$. The IFTR model is an *alternative* generalization of the TWDP model, which differs from the original FTR model proposed by the authors in [9]. The IFTR model can be applied in those situations in which the specular components follow very different paths and are affected by different scatterers.

[1]The specular components of the IFTR model are dominant components incoming from different spatial directions. As described in Durgin's seminal work [14], *examples of specular components include the direct line-of-sight wave from a transmitter antenna, the specular reflection from a flat surface in the propagation environment, or even a far-field wave diffracted from the edge of an object.*

III. Statistical characterization

We will first characterize the distribution of the received power envelope associated with the IFTR fading model, or equivalently, the distribution of the received SNR. After passing through the multipath fading channel, the signal will be affected by additive white Gaussian noise (AWGN) with one-sided power spectral density N_0. The statistical characterization of the instantaneous SNR, here denoted as γ, is crucial for the analysis and design of wireless communications systems, as many performance metrics in wireless communications are a function of the SNR.

The received average SNR $\bar{\gamma}$ after transmitting a symbol with energy density E_s undergoing a multipath fading channel as described in (1) will be

$$\begin{aligned}\bar{\gamma} &= (E_s/N_0)\,\mathbb{E}\left\{|V_r|^2\right\} = (E_s/N_0)\left(V_1^2+V_2^2+2\sigma^2\right)\\ &= (E_s/N_0)\,2\sigma^2\,(1+K)\,,\end{aligned} \tag{5}$$

where $\mathbb{E}\{\cdot\}$ denotes the expectation operator.

With all the above definitions, the chief probability functions related to the FTR fading model can now be computed.

A. MGF

In the following lemma we show that, for the IFTR fading model, it is possible to obtain the MGF of γ in closed-form.

Lemma 1: Let us consider the IFTR fading model as described in (1)-(2). Then, the MGF of the received SNR γ will be given by (6), where ${}_2F_1(\cdot)$ is the Gauss hypergeometric function [15, p. 556 (15.1.1)].

Proof: See Appendix A. ∎

When any of the parameters m_1 or m_2 takes an integer value, the MGF of the SNR in the IFTR fading model can be calculated as a finite sum of elementary functions.

Corollary 1: When $m_1 \in \mathbb{Z}^+$, the MGF of the SNR γ of the IFTR fading channel can be expressed as a finite sum of elementary terms as given in (7).

Proof: See Appendix B. ∎

Remark 1: For the case when $m_2 \in \mathbb{Z}^+$ and m_1 is not necessarily an integer, the MGF of γ can be calculated by using (7) and interchanging m_1 and m_2 and also interchanging the occurrences of $+\sqrt{1-\Delta^2}$ and $-\sqrt{1-\Delta^2}$. In the sequel, the interchanging of these parameters will also hold in the subsequent expressions obtained for $m_1 \in \mathbb{Z}^+$, when the case $m_2 \in \mathbb{Z}^+$ wants to be considered instead.

B. PDF and CDF

We now show that the PDF and CDF of the IFTR distribution can also be obtained in closed-form, provided that any of the parameters m_1 or m_2 is restricted to take a positive integer value. We note that the general case of arbitrary real m_1 and m_2 can always be numerically computed by an inverse Laplace transform over the MGF.

We derive closed-form expressions for the PDF and CDF of the SNR (or, equivalently, the power envelope) for the IFTR fading model, which will be demonstrated in the next lemma.

Lemma 2: When $m_1 \in \mathbb{Z}^+$, the PDF and CDF of the SNR γ in a FTR fading channel can be expressed in terms of the confluent hypergeometric function $\Phi_2(\cdot)$ defined in [16, p. 34, (8)], as given, respectively, in (8) and (9).

Proof: See Appendix C. ∎

Note that despite requiring the evaluation of a confluent hypergeometric function, the PDF and CDF of the IFTR fading model can be expressed in terms of a well-known function in communication theory. In fact, the $\Phi_2(\cdot)$ function also makes appearances in the CDF of common fading models such as Rician-shadowed or κ-μ shadowed [17], [18]. Moreover, this function can be efficiently evaluated using a numerical inverse Laplace transform [19]. Thus, the evaluation of the IFTR distribution functions does not pose any additional challenge compared to other state-of-the-art fading models, including the FTR fading model.

Also note that the PDF and CDF of the received signal envelope, $r = |V_r|$, can be easily derived from (8) and (9) by a simple change of variables. Specifically, we can write $f_r(r) = 2r f_\gamma(r^2)$ and $F_r(r) = F_\gamma(r^2)$, with $\bar{\gamma}$ in (8) and (9) replaced by $\Omega = \mathbb{E}\{r^2\}$. In order to illustrate the influence of the independent fluctuation of the specular components on the fading statistics, the PDF of the received signal envelope r of the IFTR and FTR models are compared for the same level of fluctuation, $m = m_1 = m_2$. Results for $m = 2$ and $m = 10$ are shown in Fig. 1. As expected, differences between both PDFs are larger for low values of m and (m_1, m_2), which correspond to larger fluctuations in the specular components, i.e., larger fading severity. As $m, m_1, m_2 \to \infty$, the fluctuation decreases and both models tend to the TWDP model.

The asymmetric fluctuation of the specular components gives the IFTR model a remarkable flexibility to change the shape of the PDF. This is shown in Fig. 2, where the PDF of the SNR is depicted for different values of m_1 and m_2 when $\Delta = 0.9$ and $\Delta = 0.1$. In all cases $K = 15$ and $\bar{\gamma} = 1$. For reference, it is also represented the PDF of the Rician-shadowed model with $m = 3$ [5]. It can be seen that, when $\Delta = 0.1$, one of the specular components dominates ($V_1 \gg V_2$) and the PDF of the IFTR distribution tends to that of the Rician-shadowed model with $m = m_1$. When $\Delta = 0.9$, both specular components have similar amplitudes and the differences with the Rician-shadowed distribution are noticeable.

The independent fluctuation of the specular components results in an increased ability of the CDF to modify its log-log convexity and concavity, even when $m_1 = m_2$. This can be observed in Fig. 3, where the CDF of the SNR for different values of the IFTR parameters are shown. The probability of severe fading is higher for $\Delta = 0.9$ because the amplitude of the specular components is similar, and therefore destructive multipath combination occurs more likely. The probability of the specular components to cancel each other is also higher for low values of m_1 and m_2, i.e., when the fluctuations are larger. In these circumstances, the influence of K is small, since the modulus of the sum $\sqrt{\zeta_1}V_1\exp(j\phi_1)+\sqrt{\zeta_2}V_2\exp(j\phi_2)$ in (1) will be generally small with respect to the power of the diffuse term, irrespective of the magnitude of $V_1^2+V_2^2$. Conversely, deep-fading probability reduces as Δ decreases, because one of the specular components becomes much larger than the other.

$$M_\gamma(s) = \frac{1+K}{1+K-\bar{\gamma}s} \frac{m_1^{m_1}}{\left[m_1 - \frac{K}{2}\left(1+\sqrt{1-\Delta^2}\right)\frac{\bar{\gamma}s}{1+K-\bar{\gamma}s}\right]^{m_1}} \frac{m_2^{m_2}}{\left[m_2 - \frac{K}{2}\left(1-\sqrt{1-\Delta^2}\right)\frac{\bar{\gamma}s}{1+K-\bar{\gamma}s}\right]^{m_2}} \times {}_2F_1\left(m_1, m_2; 1; \frac{K^2\Delta^2}{\left[2m_1\frac{1+K-\bar{\gamma}s}{\bar{\gamma}s} - K\left(1+\sqrt{1-\Delta^2}\right)\right]\left[2m_2\frac{1+K-\bar{\gamma}s}{\bar{\gamma}s} - K\left(1-\sqrt{1-\Delta^2}\right)\right]}\right). \tag{6}$$

$$M_\gamma(s) = \frac{1+K}{1+K-\bar{\gamma}s} m_1^{m_1} m_2^{m_2} \left[m_1 - \frac{K}{2}\left(1+\sqrt{1-\Delta^2}\right)\frac{\bar{\gamma}s}{1+K-\bar{\gamma}s}\right]^{m_2-m_1} \sum_{n=0}^{m_1-1} \frac{1}{n!}\binom{m_1-1}{n}\frac{\Gamma(m_2+n)}{\Gamma(m_2)} \times \left(\frac{K\Delta}{2}\frac{\bar{\gamma}s}{1+K-\bar{\gamma}s}\right)^{2n} \left[m_1 m_2 - \left(m_1\frac{K}{2}\left(1-\sqrt{1-\Delta^2}\right) + m_2\frac{K}{2}\left(1+\sqrt{1-\Delta^2}\right)\right)\frac{\bar{\gamma}s}{1+K-\bar{\gamma}s}\right]^{-m_2-n}. \tag{7}$$

$$f_\gamma(x) = \frac{1+K}{\bar{\gamma}} m_1^{m_1} m_2^{m_2} \left(m_1 + \frac{K}{2}\left(1+\sqrt{1-\Delta^2}\right)\right)^{m_2-m_1} \sum_{n=0}^{m_1-1} \frac{1}{n!}\binom{m_1-1}{n}\frac{\Gamma(m_2+n)}{\Gamma(m_2)}\left(\frac{K\Delta}{2}\right)^{2n} \times \left[m_1\frac{K}{2}\left(1-\sqrt{1-\Delta^2}\right) + m_2\frac{K}{2}\left(1+\sqrt{1-\Delta^2}\right) + m_1 m_2\right]^{-m_2-n} \times \Phi_2^{(3)}\left(n+1-m_1, m_1-m_2, m_2+n; 1; -\frac{1+K}{\bar{\gamma}}x, -\frac{m_1(1+K)}{\left(m_1+\frac{K}{2}\left(1+\sqrt{1-\Delta^2}\right)\right)\bar{\gamma}}x, -\frac{m_1 m_2(1+K)}{\left(m_1\frac{K}{2}\left(1-\sqrt{1-\Delta^2}\right) + m_2\frac{K}{2}\left(1+\sqrt{1-\Delta^2}\right) + m_1 m_2\right)\bar{\gamma}}x\right). \tag{8}$$

$$F_\gamma(x) = \frac{1+K}{\bar{\gamma}} m_1^{m_1} m_2^{m_2} \left(m_1 + \frac{K}{2}\left(1+\sqrt{1-\Delta^2}\right)\right)^{m_2-m_1} \sum_{n=0}^{m_1-1} \frac{1}{n!}\binom{m_1-1}{n}\frac{\Gamma(m_2+n)}{\Gamma(m_2)}\left(\frac{K\Delta}{2}\right)^{2n} \times \left[m_1\frac{K}{2}\left(1-\sqrt{1-\Delta^2}\right) + m_2\frac{K}{2}\left(1+\sqrt{1-\Delta^2}\right) + m_1 m_2\right]^{-m_2-n} \times x\Phi_2^{(3)}\left(n+1-m_1, m_1-m_2, m_2+n; 2; -\frac{1+K}{\bar{\gamma}}x, -\frac{m_1(1+K)}{\left(m_1+\frac{K}{2}\left(1+\sqrt{1-\Delta^2}\right)\right)\bar{\gamma}}x, -\frac{m_1 m_2(1+K)}{\left(m_1\frac{K}{2}\left(1-\sqrt{1-\Delta^2}\right) + m_2\frac{K}{2}\left(1+\sqrt{1-\Delta^2}\right) + m_1 m_2\right)\bar{\gamma}}x\right). \tag{9}$$

IV. Empirical validation

This section illustrates the capability of the IFTR fading to model the small-scale fading in quite diverse scenarios. Three types of outdoor communication links are considered: the LOS mmWave channels given in [3] and [4], the LMS channels in [5] and the UAC channels measured in [2], [20]. It will be shown that the IFTR model provides a better fit to the experimental datasets than the models previously used in each of these scenarios, and also than the FTR model.

The goodness of fit between the analytical CDF of the considered model, $F_a(x)$, and the empirical one estimated from measurements, $F_e(x)$, is quantified by using the following modified version of the Kolmogorov-Smirnov (KS) statistic:

$$\epsilon = \max_x \left|\log_{10} F_e(x) - \log_{10} F_a(x)\right|. \tag{10}$$

The logarithm in (10) is used to magnify the errors between the CDFs in the region close to zero. The rationale to overweight these values is that some of the key performance metrics of communication systems, e.g., the BER and the outage probability, are determined by the probability of deep fading events. Hence, improving the goodness of the fitting in this region is more important.

The number of parameters of the IFTR distribution to be optimized depends on the considered experimental dataset. In the mmWave and UAC channels, the empirical CDF of $x = r^2/\mathbb{E}\{r^2\}$ is given [2]–[4], [20], while the one of $x = r^2$ is reported in [5]. Hence, in addition to m_1, m_2, K and Δ, the

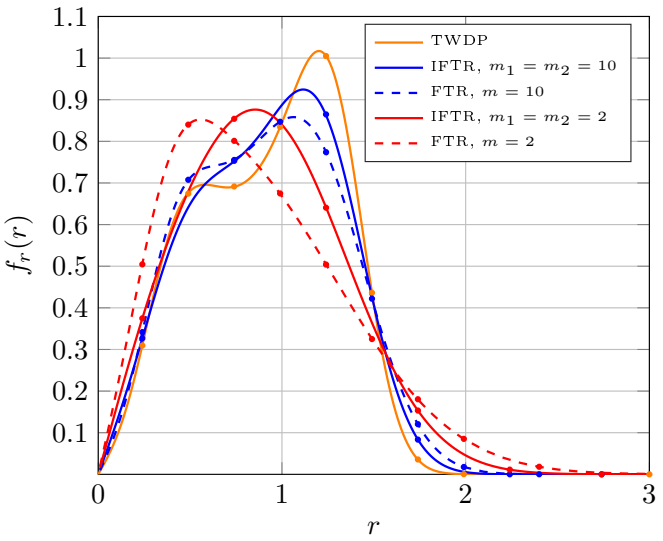

Fig. 1. PDF of the received signal envelope under FTR and IFTR fading for $K = 15$, $\Delta = 0.9$, $\Omega = 1$ and different values of $m = m_1 = m_2$. Markers correspond to simulation results.

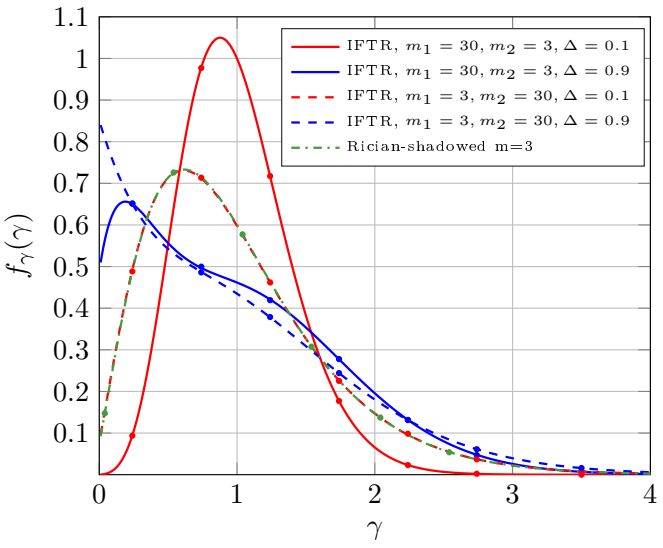

Fig. 2. PDF of the SNR under Rician-shadowed and IFTR fading with $\bar{\gamma} = 1, K = 15$ and different values of m_1, m_2 and Δ. Markers correspond to simulation results.

optimum value of $\Omega = \mathbb{E}\{r^2\}$ has to be determined also in the latter. Similar considerations apply to the remaining models included in the analysis.

A. mmWave channels

In this subsection, two outdoor LOS radio channels, measured in Brooklyn, New York, are considered at 28 GHz and 73 GHz, which will be referred to as Ch. 1 and Ch. 2, respectively. In Ch. 1, directional horn antennas were used at the transmitter and receiver in a vertical-to-horizontal cross-polarized antenna scenario. The detailed setting of the measurements for this channel can be found in [3], and the empirical CDF of the small-scale fading amplitude considered for the fitting in this work is given in [3, Fig. 6]. In Ch. 2, vertical-vertical co-

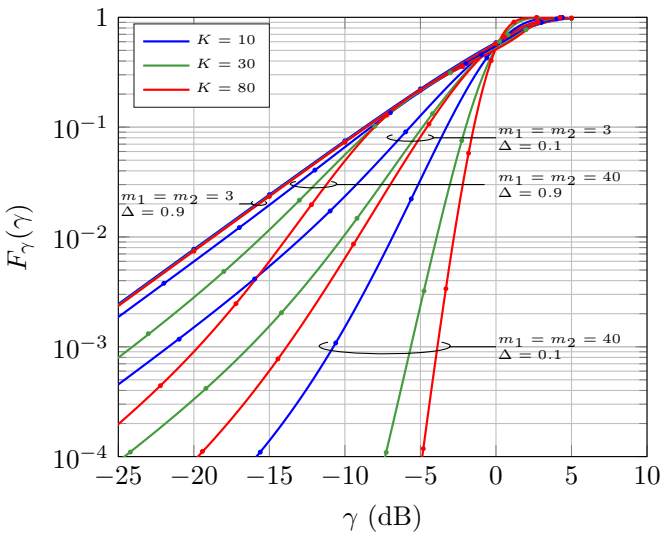

Fig. 3. CDF of the SNR under IFTR fading for $\bar{\gamma} = 1$ and different values of the model parameters. Markers correspond simulation results.

polarized pyramidal horn antennas were used, and an omni-directional antenna pattern is synthesized at the receiver. The details of the experimental setting are explained in [4], and the CDF of the fading amplitude considered in this work is given and [4, Fig. 3].

The capability of the IFTR fading to model these channels is compared to that of the Rice distribution, which has been previously used to model LOS channels in these bands. Moreover, the TWDP fading is also considered for completeness, since the analysis in [8] supports that it is favored over the Rice one. As both the IFTR and the FTR models generalize the TWDP one, the comparison is useful to assess the potential gain given by the fluctuations in the specular components in terms of fitting quality.

Table I shows the fitting error and the optimum model parameters for the aforementioned channels. For the case of Ch. 1 the IFTR fading model yields a lower error than the FTR one, which already improves the results achieved by the TWDP fading model. We see that the Rice model provides the largest error. In Ch. 2 the improvement of the IFTR model with respect to the remaining models is even higher, and is actually quite significant. The logarithmic error ϵ is 0.2068 for the IFTR model in this case, while for the other models this error is 0.3228. Since a 1-unit change in ϵ corresponds to a 10-unit change in the ratio of the empirical CDF to the analytical one, the IFTR model provides a remarkable better fit than the FTR, TWDP and Rice models for the experimental measurements considered at 73 GHz. This shows that the underlying physical assumptions of the IFTR model are closer to the real scenario than the other models. Interestingly, the TWDP and the FTR models achieve the same error as with the Rice model only in their limiting cases, i.e., $\Delta = 0$ in the TWDP model and $(\Delta = 0, m \to \infty)$ in the FTR one. This might erroneously lead to conclude that the second specular component and the LOS fluctuation are superfluous to model this channel. However, the results achieved by the IFTR fading model suggest otherwise, indicating that the consideration of

TABLE I
FITTING RESULTS FOR THE MMWAVE CHANNELS

Channel	Param.	Model			
		IFTR	FTR	TWDP	Rice
Ch. 1	ϵ	0.2203	0.2246	0.2267	0.3298
	K	476.1454	80.3916	23.1347	3.5820
	Δ	0.8463	0.5873	0.8619	-
	$(m_1, m_2)/m$	(9, 50.5)	2	-	-
Ch. 2	ϵ	0.2068	0.3228	0.3228	0.3228
	K	154.3797	45.4773	45.4773	45.4773
	Δ	0.2170	0.0000	0.0000	-
	$(m_1, m_2)/m$	(60, 3.6)	∞	-	-

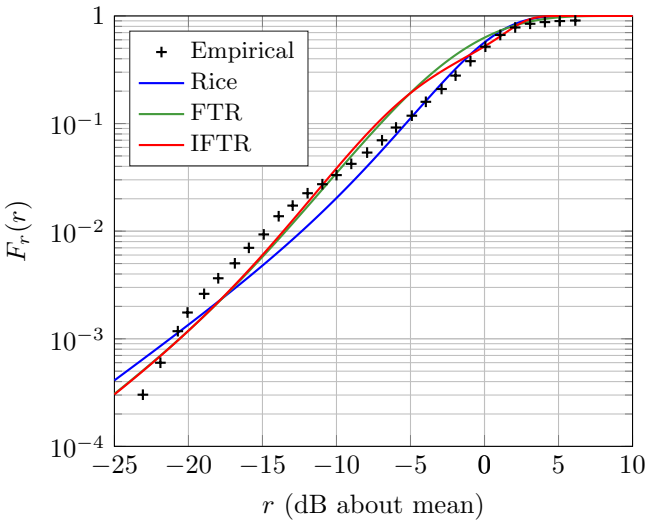

Fig. 4. Empirical and theoretical CDFs of the received signal amplitude for mmWave Ch. 1 [9, Fig. 8].

both components is beneficial as long as their fluctuation level can be independently controlled. Hence, the large value of m_1 suggests that the specular component with larger amplitude experiences almost no fluctuation (note that the variance of the fluctuations of a specular component is inversely proportional to the m parameter), i.e., ζ_1 is almost constant, while the lower amplitude component $\sqrt{\zeta_2}V_2$ fluctuates considerably.

The enhanced modeling capacity of the IFTR model can be graphically interpreted in terms of its flexibility to modify the concavity and convexity of the CDF (in a log-log scale). We illustrate this fact by reproducing the empirical and theoretical CDFs of the Rice and FTR models for Ch. 1 given in [9, Fig. 8], along with the CDF of the IFTR model. Results are shown in Fig. 4, where it can be seen that the CDF of the IFTR model is convex for $0 < r < 5$ dB, concave for r around -5 dB, and convex again for $r < -17.5$ dB.

B. LMS channels

The small-scale fading in LMS channels has been widely modeled using the Rician-shadowed distribution, where the LOS component is assumed to undergo Nakagami-m fading. The IFTR model can be seen as a generalization of the Rician-shadowed one. The capability of the IFTR fading to outperform the Rician-shadowed fading model is assessed by using the channels in [21, Fig. 1], where the empirical CDFs of two channels at 870 MHz are provided from a LMS measurement campaign carried out in rural Canada: one experiencing light shadowing due to sparse tree cover, and another one affected by heavy shadowing caused by a denser tree cover. The experimental measurements presented in this figure have also been used by other researchers (see [5] and references therein) to verify LMS models.

Table II shows the fitting results for the IFTR, FTR and Rician-shadowed models. For the sake of fairness, the parameters of the latter (denoted using the subscript RS) have been computed to minimize the error in (10), as the ones provided in [5] were obtained with a different metric. It can be seen that the IFTR model yields better fitting results than the other models for both channels. In particular, in the light shadowing channel the logarithmic error ϵ is 0.0442, which is, again, significantly lower than the error of the rest of the channels, which is 0.0507. In this light shadowing channel, the high value of m_{RS} suggests that the LOS term is essentially constant. Moreover, the FTR model achieves the error of the Rician-shadowed one only in its limiting case, $\Delta = 0$ and $m \to \infty$. These facts might again lead to conclude that a single specular component with constant amplitude suffices to adequately model this channel. In fact, the Rice distribution with $K = 3.1075$ yields the same error as these two models (although not explicitly shown in Table II). However, the values $(m_1 = 14, m_2 = 0.8)$ of the IFTR model indicate that two specular components, with considerable fluctuation in the one with lower amplitude, may be more adequate for a proper channel modeling.

The improved capability of the IFTR distribution to model the two considered channels can be graphically observed in Fig. 5, where the empirical and theoretical complementary CDFs (CCDFs) of the received signal envelope are shown. For coherence, axes have been scaled as in [5, Fig. 1]. Hence, errors have to be measured as the horizontal distance between the empirical and theoretical (logarithm of the) CCDF for a given value of the received signal level. In the heavily-shadowed channel, where all models fit the CCDF almost equally well in the low signal level region, the flexibility of the IFTR model is clearly noticeable in the high signal level region, where its CCDF changes from (log-log) convex to concave as the received signal level decreases. In the light-shadowing channel, the lower error of the IFTR model is due to its ability to achieve a better trade-off than the remaining models between the fitting in the low signal level region, where errors are overweighted, and in the high signal level zone, where they have been considered less relevant.

C. UAC channels

UAC channels in shallow waters exhibit multipath propagation and fading. The former is due to the reflections in the seabed, the surface of the sea and other objects, while the latter is caused by the surface waves (which change the reflection angles), internal waves and the motion of the communication ends, among other factors [22].

TABLE II
FITTING RESULTS FOR THE LMS CHANNELS

Channel	Parameter	Model		
		IFTR	FTR	Rician shadowed
Light shad.	ϵ	0.0442	0.0507	0.0507
	K	479.8224	4.0542	-
	$\Delta/b_{0_{\mathrm{RS}}}$	0.8290	0	0.2025
	$\Omega/\Omega_{\mathrm{RS}}$	1.6692	1.6896	1.2847
	$(m_1, m_2)\,/m/m_{\mathrm{RS}}$	(14, 0.8)	∞	100
Heavy shad.	ϵ	0.0655	0.0672	0.0673
	K	2.7457	0.7484	-
	$\Delta/b_{0_{\mathrm{RS}}}$	0.9997	0.6040	0.0429
	$\Omega/\Omega_{\mathrm{RS}}$	0.1289	0.1121	0.0258
	$(m_1, m_2)\,/m/m_{\mathrm{RS}}$	(2, 0.1)	2	100

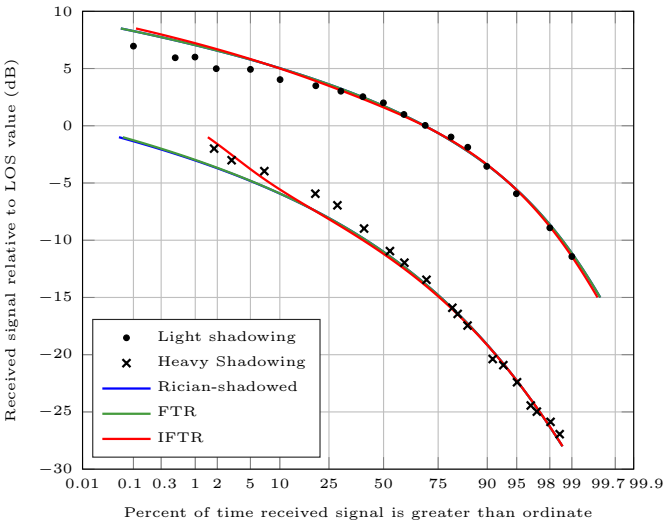

Fig. 5. Empirical and theoretical CCDFs of the received signal amplitude for the light and heavy shadowing LMS channels given in [5, Fig. 1].

The κ-μ shadowed distribution, which generalizes the Rice and Rician-shadowed ones, has been proposed to model these effects [2]. However, $\mu \in \mathbb{R}$ values are employed to this end. This considerably hinders the physical interpretation of the model (which requires $\mu \in \mathbb{Z}^+$ according to the physical model definition in [18]), and the generation of random variables for simulation purposes [18], [23]. Hence, it is of practical interest to assess its fitting capabilities also when constraining $\mu \in \mathbb{Z}^+$. It must be recalled that, for practical purposes, the IFTR model employed in this section is also constrained to have $m_1 \in \mathbb{Z}^+$, to allow for the analytical calculation of the PDF, despite random variables following the IFTR distribution can be easily generated according to (1) for non-negative real values of m_1. The same applies to the FTR model, where $m \in \mathbb{Z}^+$ is also considered.

The ability of the IFTR model to fit UAC channels is assessed by using the measurements in [2], [20]. They provide a characterization of 10 channels corresponding to links with lengths 50, 100 and 200 m, measured in Mediterranean shallow waters with a sandy seabed and depths from 14 to 30 m, approximately. The transmitter and receiver where placed at depths 3, 6 and 9 m. Sounding signals of 32, 64 and 128 kHz were transmitted. For coherence with [2], [20], channels are denoted using the nomenclature [A|B|C]D-F, where the A|B|C denotes the link length (50|100|200 m, respectively), D indicates the transmitter-receiver depth in meters and F the frequency of the transmitted signal in kHz.

The IFTR model fits these 10 channels better, i.e., the obtained logarithmic error ϵ is lower, than the $\kappa-\mu$ shadowed model with $\mu \in \mathbb{Z}^+$, except for the case of C9-32, where it yields the same error. For conciseness, only the results obtained in one channel of each length (50, 100 and 200 m) are shown in Table III, where the values corresponding to the FTR model are also shown. As in the previous scenarios, the flexibility of the IFTR fading model to control the fluctuations in each specular component independently is also exploited in this context. In channels A6-32 and B6-64 the specular component with lower amplitude is almost constant, and the component with larger amplitude exhibits considerable fluctuations. In channel C3-64, the fluctuation of the specular component with larger amplitude is much lower than the one with lower amplitude, but still considerable.

As illustrated in the previous scenarios, the independent fluctuation of the specular components results in an increased ability of the CDF to change from concave to convex, and vice-versa. This can be observed in Fig. 6, where the empirical and theoretical CDFs corresponding to channel B6-64 are shown. It can be seen that the CDF of the IFTR distribution is (log-log) concave around $r = 5$ dB, convex around $r = 0$ dB, and concave again for $r < -5$ dB.

TABLE III
FITTING RESULTS FOR THE UAC CHANNELS

Channel	Parameter	Model		
		IFTR	FTR	$\kappa-\mu$ shadowed
A6-32	ϵ	0.0569	0.0622	0.0682
	K/κ	466.2619	4.8472	1.9494
	Δ/μ	0.8720	0.9510	1
	$(m_1, m_2)\,/m/m_{\kappa-\mu}$	(2, 60)	24	1.3088
B6-64	ϵ	0.0746	0.0886	0.0758
	K/κ	508.9355	499942.1713	51.3649
	Δ/μ	0.9598	0.5256	1
	$(m_1, m_2)\,/m/m_{\kappa-\mu}$	(4, 60)	1	0.9360
C3-64	ϵ	0.1880	0.1969	0.1979
	K/κ	501.1807	5.4941	6.3239
	Δ/μ	0.5662	0	1
	$(m_1, m_2)\,/m/m_{\kappa-\mu}$	(7, 0.75)	∞	24.2813

V. PERFORMANCE ANALYSIS OF WIRELESS COMMUNICATIONS SYSTEMS

After providing a thorough empirical validation of the IFTR fading model in a number of scenarios, it is time to illustrate how the exact closed-form expressions of the statistics of the SNR can be used for performance analysis. For exemplary purposes, we calculate the BER for a family of coherent modulations, and the outage probability.

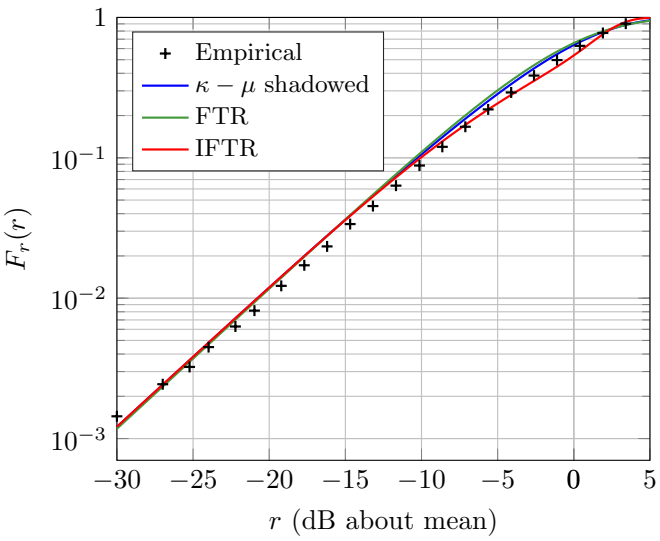

Fig. 6. Empirical and theoretical CDFs of the received signal amplitude for the B6-64 UAC channel given in [2], [20].

A. Average BER

The conditional error probability (CEP), i.e., the error rate under additive white Gaussian noise (AWGN), for many wireless communication systems with coherent detection is determined by [24]

$$P_E(\gamma) = \sum_{r=1}^{R} \alpha_r Q\left(\sqrt{\beta_r \gamma}\right), \tag{11}$$

where $Q(\cdot)$ is the Gauss Q-function and $\{\alpha_r, \beta_r\}_{r=1}^{R}$ are modulation-dependent constants.

The average error rates for the CEP given in (11) can be calculated in terms of the CDF of the SNR as [9]

$$\overline{P_e} = \sum_{r=1}^{R} \alpha_r \int_0^{\infty} \sqrt{\frac{\beta_r}{8\pi x}} e^{-\frac{\beta_r x}{2}} F_\gamma(x) dx. \tag{12}$$

Introducing (9) into (12), and with the help of [16, p. 286, (43)], a compact exact expression of the average BER can be found, as given in (13), in terms of the Lauricella function $F_D(\cdot)$ defined in [16, p. 33, (4)].

Although the derived BER expression can be easily computed using the Euler form of the F_D function, it does not provide insight about the impact of the different system parameters on performance. We now present an asymptotic, yet accurate, simple expression for the error rate in the high SNR regime. First, note that the equality in (14) holds for the asymptotic behavior of the MGF, where we write a function $a(x)$ as $o(x)$ if $\lim_{x\to\infty} a(x)/x = 0$. Thus, performing a similar approach to that in [25, Propositions 1 and 3], and after some algebraic manipulation, the asymptotic BER expression given in (15) is obtained.

B. Outage probability

The instantaneous channel capacity per unit bandwidth is well-known to be given by

$$C = \log_2(1+\gamma). \tag{16}$$

We define the outage capacity probability, or simply outage probability, as the probability that the instantaneous channel capacity C falls below a predefined threshold R_S (given in terms of rate per unit bandwidth), i.e.,

$$P_{\text{out}} = P(C < R_S) = P(\log_2(1+\gamma) < R_S). \tag{17}$$

Therefore

$$P_{\text{out}} = P\left(\gamma < 2^{R_S} - 1\right) = F_\gamma\left(2^{R_S} - 1\right). \tag{18}$$

Thus, the outage probability can be directly calculated from (9) specialized for $x = 2^{R_S} - 1$. This expression is exact and holds for all SNR values; however, it offers little insight about the effect of parameters on system performance. Fortunately, we can obtain a simple expression in the high SNR regime as follows: From (9) and [25, Proposition 5], the CDF of γ can be written as given in (19). Therefore, the outage probability can be approximated in the large SNR regime by introducing (19) into (18).

VI. Numerical results

In this section, numerical results are presented to evaluate the performance metrics of point-to-point wireless systems undergoing IFTR fading. Monte-Carlo simulations are used in all instances to validate the obtained closed-form expressions.

Figs. 7 shows the BER of the BPSK modulation versus the average SNR. Results obtained with the closed-form exact and asymptotic BER expressions given in (13) and (15) (with $R = 1$, $\alpha_1 = 1$ and $\beta_1 = 2$), respectively, are given for $K = 15$, $\Delta = 0.5$, $m_2 = 2$ and different values of m_1. BER values obtained under FTR fading with the same K, Δ and $m = m_1$ are also given as a reference, to better highlight the differences between both models. It can be seen that there is a rather good match between the asymptotic and the exact BER in the high SNR region, and performance increases when m_1 raises due to lower fading severity. Similarly, differences between the IFTR and the FTR models also increase with m_1, being about 3.6 dB for $m_1 = m = 40$. The worse (higher) BER of the IFTR fading in this case is due to the large fluctuation experienced by the specular component with amplitude V_2, which in the FTR fading is almost negligible as $m = 40$.

Fig. 8 shows the outage probability versus the average SNR for $R_s = 2$. Results are plotted for $\Delta = 0.1$ and $\Delta = 0.9$ and various combinations of m_1, m_2 and K. It can be seen that the outage probability decreases as Δ becomes lower, since in that case one specular component is much larger than the other one and it is unlikely that they cancel out each other. In these circumstances, performance also improves as m_1 increases, because the fluctuation of the largest specular component becomes smaller. It can also be noticed that the influence of K is higher for $\Delta = 0.1$, where cancellation of the specular components is unlikely.

For $\bar{\gamma} > 5$ (dB), the outage probability decreases as K increases, except for $(m_1 = 2, m_2 = 8)$ and $\Delta = 0.9$, where performance is lower for $K = 80$ than for $K = 10$. This occurs because having a destructive combination of the specular components becomes more detrimental as K increases, since almost all the received signal power is

$$\begin{aligned}\overline{P_e} = \frac{1+K}{\bar{\gamma}} m_1^{m_1} m_2^{m_2} \left(m_1 + \frac{K}{2}\left(1+\sqrt{1-\Delta^2}\right)\right)^{m_2-m_1} \sum_{n=0}^{m_1-1} \frac{1}{n!}\binom{m_1-1}{n} \frac{\Gamma(m_2+n)}{\Gamma(m_2)} \left(\frac{K\Delta}{2}\right)^{2n} \\ \times \left[m_1\frac{K}{2}\left(1-\sqrt{1-\Delta^2}\right) + m_2\frac{K}{2}\left(1+\sqrt{1-\Delta^2}\right) + m_1 m_2\right]^{-m_2-n} \sum_{r=1}^{R} \alpha_r \frac{1}{2\beta_r} \\ \times F_D^{(3)}\left(\frac{3}{2}, n+1-m_1, m_1-m_2, m_2+n; 2; -\frac{2(1+K)}{\beta_r\bar{\gamma}}, -\frac{2m_1(1+K)}{\beta_r\left(m_1+\frac{K}{2}\left(1+\sqrt{1-\Delta^2}\right)\right)\bar{\gamma}}, \right. \\ \left. -\frac{2m_1 m_2(1+K)}{\beta_r\left(m_1\frac{K}{2}\left(1-\sqrt{1-\Delta^2}\right) + m_2\frac{K}{2}\left(1+\sqrt{1-\Delta^2}\right) + m_1 m_2\right)\bar{\gamma}}\right).\end{aligned} \tag{13}$$

$$\begin{aligned}|M_\gamma(s)| = \frac{1+K}{\bar{\gamma}|s|} \frac{m_1^{m_1}}{\left[m_1+\frac{K}{2}\left(1+\sqrt{1-\Delta^2}\right)\right]^{m_1}} \frac{m_2^{m_2}}{\left[m_2+\frac{K}{2}\left(1-\sqrt{1-\Delta^2}\right)\right]^{m_2}} \\ \times {}_2F_1\left(m_1, m_2; 1; \frac{K^2\Delta^2}{\left[2m_1+K\left(1+\sqrt{1-\Delta^2}\right)\right]\left[2m_2+K\left(1-\sqrt{1-\Delta^2}\right)\right]}\right) + o\left(|s|^{-1}\right).\end{aligned} \tag{14}$$

$$\begin{aligned}\overline{P_e} \approx \frac{1+K}{2\bar{\gamma}} \frac{m_1^{m_1}}{\left[m_1+\frac{K}{2}\left(1+\sqrt{1-\Delta^2}\right)\right]^{m_1}} \frac{m_2^{m_2}}{\left[m_2+\frac{K}{2}\left(1-\sqrt{1-\Delta^2}\right)\right]^{m_2}} \left(\sum_{r=1}^{R}\frac{\alpha_r}{\beta_r}\right) \\ \times {}_2F_1\left(m_1, m_2; 1; \frac{K^2\Delta^2}{\left[2m_1+K\left(1+\sqrt{1-\Delta^2}\right)\right]\left[2m_2+K\left(1-\sqrt{1-\Delta^2}\right)\right]}\right), \quad \bar{\gamma} \gg 1.\end{aligned} \tag{15}$$

$$\begin{aligned}F_\gamma(x) = \frac{1+K}{\bar{\gamma}} \frac{m_1^{m_1}}{\left[m_1+\frac{K}{2}\left(1+\sqrt{1-\Delta^2}\right)\right]^{m_1}} \frac{m_2^{m_2}}{\left[m_2+\frac{K}{2}\left(1-\sqrt{1-\Delta^2}\right)\right]^{m_2}} \\ \times {}_2F_1\left(m_1, m_2; 1; \frac{K^2\Delta^2}{\left[2m_1+K\left(1+\sqrt{1-\Delta^2}\right)\right]\left[2m_2+K\left(1-\sqrt{1-\Delta^2}\right)\right]}\right) x + o\left(\bar{\gamma}^{-1}\right).\end{aligned} \tag{19}$$

conveyed by the specular components as $K \to \infty$. When $\Delta < 1$, the probability of destructive sum depends on the specific fluctuation of the specular components, and becomes larger as the fluctuation of the larger specular component increases, i.e., m_1 decreases. This is reflected by the fact that the outage probability is higher for $(m_1 = 2, m_2 = 8)$ than for $(m_1 = 8, m_2 = 2)$. The asymmetry in the fluctuation of the specular components becomes immaterial when $\Delta = 1$, where $(m_1 = 2, m_2 = 8)$ and $(m_1 = 8, m_2 = 2)$ yielding the same outage probabilities (not explicitly shown in Fig. 8).

VII. Conclusion and remarks

In this work, a new small-scale fading model consisting of two specular (dominant) components with independent fluctuation plus a diffuse term has been introduced for the first time in the literature. We provide closed-form expressions for the PDF, CDF and MGF of the received SNR. Also, the outage probability and the error performance of wireless communication systems over channels with IFTR fading have been obtained in closed-form.

The chief probability functions of the received SNR are expressed in terms of functions used in other state-of-the-art fading models and are given in terms of only four parameters with direct physical interpretation: $K \geq 0$, which quantifies the ratio of the average power of the specular components to the power of the diffuse term; $\Delta \in [0, 1]$, which measures the similarity between the average power of the specular components, with $\Delta = 1$ representing the case where both components are equal and $\Delta = 0$ the case in which one of them is zero; and $m_1, m_2 > 0$, which determine the extent of the fluctuation of each specular component, with lower variations as $m_1, m_2 \to \infty$. The IFTR fading model generalizes previous models such as the Rice (obtained when $m_1, m_2 \to \infty$ and $\Delta = 0$), Rician-Shadowed (resulting when $\Delta = 0$), TWDP (when $m_1, m_2 \to \infty$) and others. It also innovates on the FTR model, whose specular components jointly fluctuate, as opposed to the dissimilar fluctuations of the IFTR model.

The joint values of the model parameters determine the received signal level. Thus, enlarging the value of K reduces

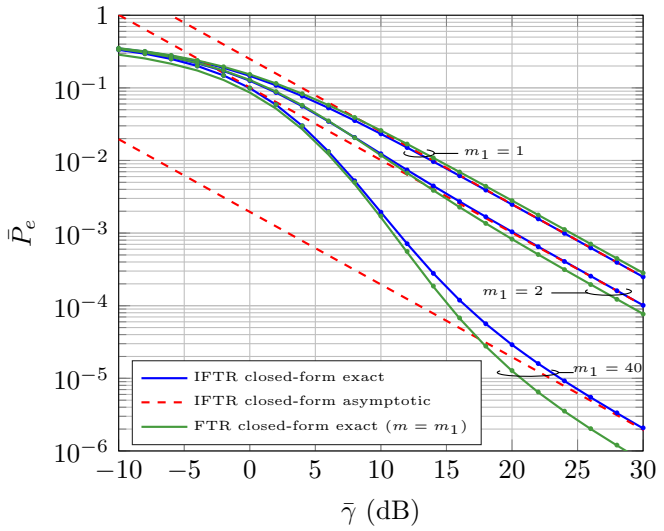

Fig. 7. Exact and asymptotic closed-form BER vs. average SNR for BPSK modulation under IFTR and FTR fading with $K = 15$, $\Delta = 0.5$, $m_2 = 2$ and different values of $m_1 = m$. Markers denote results obtained using Monte-Carlo simulations.

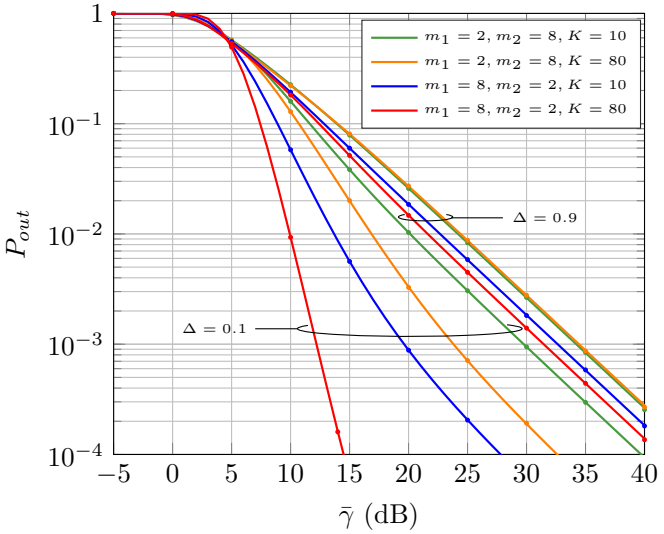

Fig. 8. Outage probability vs. average SNR for $R_s = 2$ and different combinations of $m, 1, m_2, K$ and Δ. Markers denote results obtained using Monte-Carlo simulations.

the probability of severe fading. However, its influence is relevant only if the specular components have dissimilar powers ($\Delta \to 0$) and almost no fluctuation ($m_1, m_2 \to \infty$). As ($\Delta \to 1$), the amplitude of the specular components becomes similar, and destructive multipath combination is more probable to occur. Similarly, as m_1, m_2 decrease, the fluctuations of these components increase and then the reception of lower values becomes more likely. The dissimilar fluctuations of the specular components introduced by the IFTR model provides an additional degree of freedom compared to the original FTR model. The effect of such independent fluctuations is more prominent when the components have notably different average power ($\Delta \to 0$), and it provides an increased flexibility to change the log-log concavity and convexity of the CDF. Moreover, the dissimilar fluctuations of the specular components have a clear physical interpretation, as it models the case where the dominant waves follow very different paths and are affected by different scatterers and/or perturbations. The presented results suggest that this situation is quite common in rather diverse scenarios such as LOS mmWave, LMS and UAC channels.

The error, in a logarithmic scale, between the analytical CDF of the IFTR model and the empirical one estimated from measurements in the referred scenarios has been computed, and results were compared to those of the FTR model as well as other models typically used in each of the different considered scenarios. In all the presented cases, the IFTR outperforms the other models, providing a better fit. Moreover, we have shown that the improvement of the IFTR model with respect to the compared models is remarkable in LOS scenarios when there is a direct path between transmitter and receiver, through which the signal has negligible fluctuations, and an additional dominant reflected wave is also received experiencing strong fluctuations. This significant improvement can be explained by the fact that such different fluctuations of the two dominant components suggests that they are highly uncorrelated, thus closely matching the physical assumptions of the IFTR model.

Appendix A
Proof of Lemma 1

Let us consider the fading channel model given in (1) conditioned to a particular realization $\zeta_1 = u_1$, $\zeta_2 = u_2$ of the random variables modeling the fluctuation of the specular components. In this case, we can write

$$V_r|_{u_1,u_2} = \sqrt{u}_1 V_1 \exp(j\phi_1) + \sqrt{u}_2 V_2 \exp(j\phi_2) + X + jY. \tag{20}$$

This corresponds to the classical TWDP fading model where the amplitudes of the specular components are given by $\sqrt{u}_1 V_1$ and $\sqrt{u}_2 V_2$, for which the following ancillary parameters can be defined:

$$K_{u_1,u_2} = \frac{u_1 V_1^2 + u_2 V_2^2}{2\sigma^2}, \tag{21}$$

$$\Delta_{u_1,u_2} = \frac{2\sqrt{u_1 u_2} V_1 V_2}{u_1 V_1^2 + u_2 V_2^2}. \tag{22}$$

The conditional average SNR for the fading model described in (20) will be

$$\begin{aligned} \bar{\gamma}_{u_1,u_2} &= (E_s/N_0)\left(u_1 V_1^2 + u_2 V_2^2 + 2\sigma^2\right) \\ &= (E_s/N_0)\, 2\sigma^2 \left(1 + K_{u_1,u_2}\right). \end{aligned} \tag{23}$$

The MGF of the TWDP fading model was shown in [7] to be given in closed-form as

$$\begin{aligned} M_{\gamma_{u_1,u_2}}(s) = &\frac{1 + K_{u_1,u_2}}{1 + K_{u_1,u_2} - \bar{\gamma}_{u_1,u_2} s} \\ &\times \exp\left(\frac{K_{u_1,u_2}\bar{\gamma}_{u_1,u_2} s}{1 + K_{u_1,u_2} - \bar{\gamma}_{u_1,u_2} s}\right) \\ &\times I_0\left(\frac{\Delta_{u_1,u_2} K_{u_1,u_2}\bar{\gamma}_{u_1,u_2} s}{1 + K_{u_1,u_2} - \bar{\gamma}_{u_1,u_2} s}\right), \end{aligned} \tag{24}$$

where $I_0(\cdot)$ is the zero-order modified Bessel function of the first kind [15, p. 375 (9.6.12)]. Note that, from (5) and (23), we can write

$$\frac{1+K_{u_1,u_2}}{\bar{\gamma}_{u_1,u_2}} = \frac{1}{(E_s/N_0)\,2\sigma^2} = \frac{1+K}{\bar{\gamma}}, \tag{25}$$

and thus, we have

$$\begin{aligned} M_{\gamma_{u_1,u_2}}(s) &= \frac{\frac{1+K_{u_1,u_2}}{\bar{\gamma}_{u_1,u_2}}}{\frac{1+K_{u_1,u_2}}{\bar{\gamma}_{u_1,u_2}} - s} \exp\left(\frac{K_{u_1,u_2}s}{\frac{1+K_{u_1,u_2}}{\bar{\gamma}_{u_1,u_2}} - s}\right) \\ &\quad \times I_0\left(\Delta_{u_1,u_2}\frac{K_{u_1,u_2}s}{\frac{1+K_{u_1,u_2}}{\bar{\gamma}_{u_1,u_2}} - s}\right) \\ &= \frac{\frac{1+K}{\bar{\gamma}}}{\frac{1+K}{\bar{\gamma}} - s} \exp\left(\frac{K_{u_1,u_2}s}{\frac{1+K}{\bar{\gamma}} - s}\right) \\ &\quad \times I_0\left(\Delta_{u_1,u_2}\frac{K_{u_1,u_2}s}{\frac{1+K}{\bar{\gamma}} - s}\right) \\ &= \frac{1+K}{1+K-\bar{\gamma}s} \exp\left(\frac{K_{u_1,u_2}\bar{\gamma}s}{1+K-\bar{\gamma}s}\right) \\ &\quad \times I_0\left(\Delta_{u_1,u_2}\frac{K_{u_1,u_2}\bar{\gamma}s}{1+K-\bar{\gamma}s}\right) \\ &= \mathcal{B}(s)\exp\left(K_{u_1,u_2}\mathcal{A}(s)\right) I_0\left(\Delta_{u_1,u_2}K_{u_1,u_2}\mathcal{A}(s)\right), \end{aligned} \tag{26}$$

where we have defined

$$\mathcal{A}(s) \triangleq \frac{\bar{\gamma}s}{1+K-\bar{\gamma}s}, \qquad \mathcal{B}(s) \triangleq \frac{1+K}{1+K-\bar{\gamma}s}. \tag{27}$$

Considering that

$$\begin{aligned} \Delta_{u_1,u_2}K_{u_1,u_2} &= \frac{2\sqrt{u_1u_2}V_1V_2}{u_1V_1^2+u_2V_2^2}\frac{u_1V_1^2+u_2V_2^2}{2\sigma^2} \\ &= \sqrt{u_1u_2}\frac{V_1V_2}{\sigma^2}, \end{aligned} \tag{28}$$

and using (21), the conditional MGF can be written as

$$\begin{aligned} M_{\gamma_{u_1,u_2}}(s) &= \mathcal{B}(s)\exp\left(u_1\frac{V_1^2}{2\sigma^2}\mathcal{A}(s)\right)\exp\left(u_2\frac{V_2^2}{2\sigma^2}\mathcal{A}(s)\right) \\ &\quad \times I_0\left(\sqrt{u_1u_2}\frac{V_1V_2}{\sigma^2}\mathcal{A}(s)\right). \end{aligned} \tag{29}$$

The MGF of the SNR of the IFTR model can be obtained by averaging (29) over all possible realizations of the random variables ζ_1 and ζ_2, i.e.

$$M_\gamma(s) = \int_0^\infty\int_0^\infty M_{\gamma_{u_1,u_2}}(s) f_{\zeta_1}(u_1) f_{\zeta_2}(u_2)\,du_1du_2, \tag{30}$$

where $f_{\zeta_i}(\cdot)$ is given in (2). The double integral in (30) can be solved in closed-form by iteratively integrating with respect to variables u_1 and u_2. Thus, we can write

$$\begin{aligned} M_\gamma(s) &= \mathcal{B}(s)\frac{m_1^{m_1}}{\Gamma(m_1)}\frac{m_2^{m_2}}{\Gamma(m_2)}\int_0^\infty u_2^{m_2-1} \\ &\quad \times \exp\left[-u_2\left(m_2 - \frac{V_2^2}{2\sigma^2}\mathcal{A}(s)\right)\right]\mathcal{I}(u_2)du_2, \end{aligned} \tag{31}$$

where we have defined

$$\begin{aligned} \mathcal{I}(u_2) &\triangleq \int_0^\infty u_1^{m_1-1}\exp\left[-u_1\left(m_1 - \frac{V_1^2}{2\sigma^2}\mathcal{A}(s)\right)\right] \\ &\quad \times I_0\left(\sqrt{u_1u_2}\frac{V_1V_2}{\sigma^2}\mathcal{A}(s)\right)du_1, \end{aligned} \tag{32}$$

which can be calculated, using [26, eqs. (6.643.2) and (9.220.2)], as

$$\begin{aligned} \mathcal{I}(u_2) &= \frac{\Gamma(m_1)}{\left[m_1 - \frac{V_1^2}{2\sigma^2}\mathcal{A}(s)\right]^{m_1}} \\ &\quad \times {}_1F_1\left(m_1;1;u_2\frac{\frac{V_1^2}{2\sigma^2}\frac{V_2^2}{2\sigma^2}\mathcal{A}^2(s)}{m_1 - \frac{V_1^2}{2\sigma^2}\mathcal{A}(s)}\right), \end{aligned} \tag{33}$$

where ${}_1F_1(\cdot)$ is the Kummer confluent hypergeometric function [15, p. 504 (13.1.2)]. Introducing (33) into (31) we obtain, with the help of [26, eq. (7.621.4)],

$$\begin{aligned} M_\gamma(s) &= \mathcal{B}(s)\frac{m_1^{m_1}}{\left[m_1 - \frac{V_1^2}{2\sigma^2}\mathcal{A}(s)\right]^{m_1}}\frac{m_2^{m_2}}{\left[m_2 - \frac{V_2^2}{2\sigma^2}\mathcal{A}(s)\right]^{m_2}} \\ &\quad \times {}_2F_1\left(m_2, m_1; 1; \frac{\frac{V_1^2}{2\sigma^2}\frac{V_2^2}{2\sigma^2}\mathcal{A}^2(s)}{\left[m_1 - \frac{V_1^2}{2\sigma^2}\mathcal{A}(s)\right]\left[m_2 - \frac{V_2^2}{2\sigma^2}\mathcal{A}(s)\right]}\right). \end{aligned} \tag{34}$$

Considering now that, from (3) and (4),

$$\frac{V_1^2}{2\sigma^2} = \frac{K}{2}\left(1+\sqrt{1-\Delta^2}\right), \ \frac{V_2^2}{2\sigma^2} = \frac{K}{2}\left(1-\sqrt{1-\Delta^2}\right), \tag{35}$$

we finally obtain (6).

Appendix B
Proof of Corollary 1

For $m \in \mathbb{Z}^+$ the Kummer hypergeometric function can be expressed in terms of the Laguerre polynomials by using [27, eq. 24], and from the well-known Kummer transformation we have

$${}_1F_1(m,1;z) = e^z\sum_{n=0}^{m-1}\binom{m-1}{n}\frac{z^n}{n!}. \tag{36}$$

Thus, for $m_1 \in \mathbb{Z}^+$, the function $\mathcal{I}(\cdot)$ given in (33) can be written as

$$\begin{aligned} \mathcal{I}(u_2) &= \frac{\Gamma(m_1)}{\left[m_1 - \frac{V_1^2}{2\sigma^2}\mathcal{A}(s)\right]^{m_1}}\exp\left(u_2\frac{\frac{V_1^2}{2\sigma^2}\frac{V_2^2}{2\sigma^2}\mathcal{A}^2(s)}{m_1 - \frac{V_1^2}{2\sigma^2}\mathcal{A}(s)}\right) \\ &\quad \times \sum_{n=0}^{m_1-1}\frac{1}{n!}\binom{m_1-1}{n}\left(u_2\frac{\frac{V_1^2}{2\sigma^2}\frac{V_2^2}{2\sigma^2}\mathcal{A}^2(s)}{m_1 - \frac{V_1^2}{2\sigma^2}\mathcal{A}(s)}\right)^n. \end{aligned} \tag{37}$$

Introducing (37) into (31) the resulting integral can be solved in closed-form, yielding (7) after some manipulation.

APPENDIX C
PROOF OF LEMMA 2

The MGF of γ given in (7) can be factorized as

$$\begin{aligned} M_\gamma(s) = &-(1+K)\, m_1^{m_1} m_2^{m_2} a_1^{m_1-m_2} \sum_{n=0}^{m_1-1} \frac{1}{n!} \\ &\times \binom{m_1-1}{n} \frac{\Gamma(m_2+n)}{\Gamma(m_2)} \left(\frac{K\Delta}{2}\right)^2 \frac{1}{a_2^{m_2+n}} \frac{1}{\bar{\gamma}s} \\ &\times \left(1-\frac{1+K}{\bar{\gamma}s}\right)^{m_1-n-1} \left(1-\frac{m_1(1+K)}{a_1\bar{\gamma}s}\right)^{m_2-m_1} \\ &\times \left(1-\frac{m_1 m_2(1+K)}{a_2\bar{\gamma}s}\right)^{-(m_2+n)}, \end{aligned} \tag{38}$$

where we have defined

$$\begin{aligned} a_1 &\triangleq m_1 + \frac{K}{2}\left(1+\sqrt{1-\Delta^2}\right) \\ a_2 &\triangleq m_1 \frac{K}{2}\left(1-\sqrt{1-\Delta^2}\right) \\ &\quad + m_2 \frac{K}{2}\left(1+\sqrt{1-\Delta^2}\right) + m_1 m_2. \end{aligned} \tag{39}$$

Taking into account that the PDF is related to the MGF by the inverse Laplace transform, i.e., $f_\gamma(x) = \mathcal{L}^{-1}[M_\gamma(-s); x]$, (8) follows from (38) and the Laplace transform pair given in [16, p. 290, (55)]. On the other hand, (9) is obtained analogously by considering that $F_\gamma(x) = \mathcal{L}^{-1}[M_\gamma(-s)/s; x]$.

REFERENCES

[1] C.-X. Wang, J. Huang, H. Wang, S. Gao, X. You, and Y. Hao, "6G wireless channels measurements and models: trends and challenges," *IEEE Veh. Technol. Mag.*, vol. 15, no. 4, pp. 22–32, Dec. 2020.

[2] F. J. Cañete, J. López-Fernández, C. García-Corrales, A. Sánchez, E. Robles, F. J. Rodrigo, and J. F. Paris, "Measurement and modeling of narrowband channels for ultrasonic underwater communications," *Sensors*, vol. 16, no. 2, p. 256, 2016.

[3] M. K. Samimi, G. R. MacCartney, S. Sun, and T. S. Rappaport, "28 GHz Millimeter-Wave Ultrawideband Small-Scale Fading Models in Wireless Channels," in *Proc. 2016 IEEE 83rd Vehicular Technology Conference (VTC Spring)*, May 2016.

[4] S. Sun, H. Yan, G. R. MacCartney Jr., and T. S. Rappaport, "Millimeter wave small-scale spatial statistics in an urban microcell scenario," in *Proc. IEEE International Conference on Communications (ICC)*, 2017, pp. 1–7.

[5] A. Abdi, W. Lau, M.-S. Alouini, and M. Kaveh, "A new simple model for land mobile satellite channels: first- and second-order statistics," *IEEE Trans. Wireless Commun.*, vol. 2, no. 3, pp. 519–528, May 2003.

[6] G. D. Durgin, T. S. Rappaport, and D. A. de Wolf, "New analytical models and probability density functions for fading in wireless communications," *IEEE Trans. Commun.*, vol. 50, no. 6, pp. 1005–1015, June 2002.

[7] M. Rao, F. J. Lopez-Martinez, M.-S. Alouini, and A. Goldsmith, "MGF Approach to the Analysis of Generalized Two-Ray Fading Models," *IEEE Trans. Wireless Commun.*, vol. 14, no. 5, pp. 2548–2561, May 2015.

[8] E. Zöchmann, S. Caban, C. F. Mecklenbräuker, S. Pratschner, M. Lerch, S. Schwarz, and M. Rupp, "Better than Rician: modelling millimetrewave channels as two-wave with diffuse power," *Eurasip J. Wirel. Commun. Netw.*, vol. 2019, no. 1, pp. 1–17, 2019.

[9] J. M. Romero-Jerez, F. J. Lopez-Martinez, J. F. Paris, and A. J. Goldsmith, "The fluctuating two-ray fading model: Statistical characterization and performance analysis," *IEEE Trans. Wireless Commun.*, vol. 16, no. 7, pp. 4420–4432, Jul. 2017.

[10] M. Olyaee, M. Eslami, J. Haghighat, and W. Hamouda, "Performance Analysis of Cellular Downlink With Fluctuating Two-Ray Channels Under Inter-Cell Interference," *IEEE Trans. Veh. Technol.*, vol. 69, no. 11, pp. 13 437–13 449, 2020.

[11] C. Yin, G. Giunta, D. Orlando, C. Hao, and C. Hou, "A channel classification scheme accounting for nakagami-m shadowing and ftr model," *IEEE Wireless Commun. Lett.*, vol. 10, no. 10, pp. 2289–2293, 2021.

[12] B. Shi, L. Pallotta, G. Giunta, C. Hao, and D. Orlando, "Parameter estimation of fluctuating two-ray model for next generation mobile communications," *IEEE Trans. Veh. Technol.*, vol. 69, no. 8, pp. 8684–8697, 2020.

[13] J. Wang, H. Zhou, Y. Li, Q. Sun, Y. Wu, S. Jin, T. Q. Quek, and C. Xu, "Wireless channel models for maritime communications," *IEEE Access*, vol. 6, pp. 68 070–68 088, 2018.

[14] G. D. Durgin, "Theory of stochastic local area channel modeling for wireless communications," Ph.D. dissertation, Virginia Polytechnic Institute and State University, 2000.

[15] M. Abramowitz and I. A. Stegun, *Handbook of mathematical functions with formulas, graphs, and mathematical tables*. 9th ed. New York, NY: Dover Publications, Dec. 1970.

[16] P. W. K. H. M. Srivastava, *Multiple Gaussian Hypergeometric Series*. John Wiley & Sons, 1985.

[17] J. F. Paris, "Closed-form expressions for Rician shadowed cumulative distribution function," *Electron. Lett.*, vol. 46, no. 13, pp. 952–953, June 2010.

[18] ——, "Statistical Characterization of κ-μ Shadowed Fading," *IEEE Trans. Veh. Technol.*, vol. 63, no. 2, pp. 518–526, Feb 2014.

[19] E. Martos-Naya, J. M. Romero-Jerez, F. J. Lopez-Martinez, and J. F. Paris, "A MATLAB program for the computation of the confluent hypergeometric function Φ_2," *Technical Report, Universidad de Malaga*, 2016. [Online]. Available: http://hdl.handle.net/10630/12068

[20] A. Sánchez, E. Robles, F. Rodrigo, F. Ruiz-Vega, U. Fernández-Plazaola, and J. Paris, "Measurement and modeling of fading in ultrasonic underwater channels," in *Proc. 2nd International Conference and Exhibition on Underwater Acoustic*, Rhodes (Greece), Jun. 2014, pp. 1–6.

[21] C. Loo, "A statistical model for a land mobile satellite link," *IEEE Trans. Veh. Technol.*, vol. 34, no. 3, pp. 122–127, 1985.

[22] P. A. van Walree, "Propagation and scattering effects in inderwater acoustc communication channels," *IEEE J. Ocean. Eng.*, vol. 38, no. 4, pp. 614–631, Oct. 2013.

[23] M. Yacoub, "The κ-μ distribution and the η-μ distribution," *IEEE Antennas Propag. Mag.*, vol. 49, no. 1, pp. 68–81, Feb 2007.

[24] F. J. Lopez-Martinez, E. Martos-Naya, J. F. Paris, and U. Fernández-Plazaola, "Generalized BER analysis of QAM and its application to MRC under imperfect CSI and interference in Ricean fading channels," *IEEE Trans. Veh. Technol.*, vol. 59, no. 5, pp. 2598–2604, June 2010.

[25] Z. Wang and G. Giannakis, "A simple and general parameterization quantifying performance in fading channels," *IEEE Trans. Commun.*, vol. 51, no. 8, pp. 1389–1398, Aug. 2003.

[26] I. S. Gradshteyn and I. M. Ryzhik, *Table of Integrals, Series and Products*, 7th ed. Academic Press Inc, 2007.

[27] A. Erdélyi, "Transformation of a certain series of products of confluent hypergeometric functions. Applications to Laguerre and Charlier polynomials," *Compositio Mathematica*, vol. 7, pp. 340–352, 1940.

Maryam Olyaee received the B.Sc. degree in electrical engineering from the University of Shahed, Tehran, Iran, in 2014, and the M.Sc. and Ph.D. degrees in electrical engineering from the Shiraz University of Technology, Shiraz, Iran, in 2016 and 2021, respectively. She has been an Assistant Researcher at the University of Malaga, Spain, from March 2021 to August 2022, and she is currently a Research Fellow at the University of Granada, Spain, from September 2022. She has participated in different research projects on topics related to secure wireless communications, radio channel modeling for millimeter-wave communications and performance analysis of wireless communications systems. Her research interests include wireless and cellular communications, multiuser MIMO/MIMO-OFDM, massive MIMO systems, RIS, green communications, wireless channel modeling, and mm-Wave communications for 5G and beyond.

José A. Cortés received the M.S. and Ph.D. degrees in telecommunication engineering from the Universidad de Málaga, Spain, in 1998 and 2007, respectively. In 1999, he was with Alcatel España R&D. He joined the Communication Engineering Department, Universidad de Málaga, in 1999, where he became an Associate Professor in 2010. From 2000 to 2002, he collaborated with the Nokia System Competence Team in Málaga. From 2014 to 2016 he was on a leave of absence working as a consultant on the development of Atmel's power line communications (PLC) solutions. He was the general co-chair of the IEEE ISPLC 2020. He is associate editor of the IEEE Open Journal of the Communications Society, where he has been recognized as exemplary editor in 2021. He served as associate editor of the IEEE Communications Letters, where he has been recognized as exemplary editor in 2019, 2020 and 2021. He serves as chair of the IEEE Communications Society Technical Committee on Power Line Communications since 2022. His research interests include digital signal processing for communications, mainly focused on channel characterization and transmission techniques for PLC.

F. Javier López-Martínez (Senior Member, IEEE) received the M.Sc. and Ph.D. degrees in telecommunication engineering from the University of Malaga, Spain, in 2005 and 2010, respectively. He was a Marie Curie Postdoctoral Fellow at the Wireless Systems Laboratory, Stanford University, from 2012 to 2014. He was a Visiting Researcher at the University College London, in 2010, and Queen's University Belfast, in 2018. He is an Associate Professor (on leave) with the Communication Engineering Department, University of Malaga, and an EMERGIA Research Professor with the Department of Signal Theory, Networking and Communications, University of Granada.

He has received several research awards, including the Best Paper Award from the Communication Theory Symposium at the IEEE Globecom 2013, the Outstanding Service Award by the IEEE Communication Theory Technical Committee in 2022, the IEEE COMMUNICATIONS LETTERS Exemplary Reviewer Certificate, in 2014 and 2019, and the IEEE TRANSACTIONS ON COMMUNICATIONS Exemplary Reviewer Certificate, in 2014, 2016, and 2019. His research interests include wireless channel modeling, physical layer security, and signal processing for communications. He was an Editor of the IEEE TRANSACTIONS ON COMMUNICATIONS, in the area of wireless communications, from 2017 to 2022.

José F. Paris received his MSc and PhD degrees in Telecommunication Engineering from the University of Málaga, Spain, in 1996 and 2004, respectively. In 1997, he joined the University of Málaga where he is now a Full Professor of Signal Theory and Communications. His teaching activities include several courses on digital communications, signal processing and acoustic engineering. His research interests are related to wireless communications and statistical signal processing. In 2005, he spent five months as a Visitor Associate Professor at Stanford University with Prof. Andrea J. Goldsmith.

In 2016 he received the IEEE Neal Shepherd Memorial Best Propagation Paper Award of the IEEE Vehicular Technology Society for the κ-μ shadowed fading model proposal. He is also co-inventor of two other popular models: the Málaga-$\mathcal{M}$ model for optical scintilliation and the FTR fading model. He has served as Editor of IEEE Communications Letters and IEEE Transactions on Vehicular Technology.

Juan M. Romero-Jerez (Senior Member, IEEE) received the B.Sc/M.Sc. degrees in telecommunications engineering and also in mathematics from the University of Malaga, Spain, and the Ph.D. degree in telecommunications engineering from the University of Malaga, in 2001. In 1996, he joined the Department of Electronic Technology, University of Malaga, where he is currently a Full Professor. He was a Visiting Associate Professor with the Department of Electrical Engineering, Stanford University, Stanford, CA, USA, from September 2005 to February 2006, September 2007 to February 2008, and February 2016 to March 2016. He has participated in several research projects in the areas of packet radio transmission, multiple antennas, interference management, and cellular networks. His current research interests include the area of wireless communications and more specifically: wireless communications performance analysis, multipath fading, wireless channel modeling, diversity systems, smart antennas, MIMO performance, and interference management. He was an Editor of the IEEE TRANSACTIONS ON WIRELESS COMMUNICATIONS from 2015 to 2020.